

Pressure-induced structural phase transitions in a two-dimensional system

Pablo F. Damasceno, Luis Gustavo V. Gonçalves, and José Pedro Rino*

Departamento de Física, Universidade Federal de São Carlos, 13.565-905, São Carlos, São Paulo, Brazil

Rita de Cássia M. T. de Oliveira

Escola Superior de Tecnologia, Universidade do Estado do Amazonas, 69.077-000, Manaus, Amazonas, Brazil

(Received 30 June 2008; revised manuscript received 1 December 2008; published 20 March 2009)

We have performed molecular-dynamics simulation to analyze structural phase transitions in a two-dimensional system using a model which has been proposed to study pressure-induced martensitic transformation in iron. At low temperatures, the square \leftrightarrow hexagonal phase transition was observed at $P^*=5.4(1)$ and the reverse transition occurred only by application of tension on the system. At a temperature near the melting point, the hexagonal phase was reached at $P^*=3.1(1)$ and it went back to square symmetry at $P^*=1.9(1)$ showing hysteresis. The activation energy for this transition was evaluated using the nudged elastic band method. Our work permitted to detail the mechanism of square \leftrightarrow hexagonal transformations, contributing for a better understanding about the dynamics of self-organization phenomenon.

DOI: [10.1103/PhysRevB.79.104109](https://doi.org/10.1103/PhysRevB.79.104109)

PACS number(s): 64.60.-i

I. INTRODUCTION

The study of pressure-induced phase transitions has received much attention in these days. The development of computational tools has supported theoreticians to better understand the mechanisms involved in structural phase transitions. Special interest has been devoted to the studies of the high pressure effect in the mantle core of the Earth. For example, recent experiments and theoretical calculation proposed that iron present in the Earth's core is stable in a body-centered-cubic (bcc) phase.¹⁻⁵ In order to elucidate the atomic pathway of the iron under pressure, Lee *et al.*⁶ used molecular dynamics (MD) to determine how the particles move relatively to one another during its pressure-induced structural transitions. Lee managed to confirm the model proposed by Mao *et al.*⁷ that explains that, by increasing pressure, the bcc structure transforms to the hcp structure by contraction along the $[001]$ direction combined with sliding along the $[\bar{1}10]$ and $[1\bar{1}0]$ directions for alternate (110) planes. Besides these hard-core three-dimensional (3D) systems, soft matter, such as colloidal inclusion in thin films, is a typical example of two-dimensional (2D) system. Recently, the fabrication of structures by self-assembly method permitted scientists to obtain several symmetric and ordered conformations.⁸⁻¹² The spontaneous formations of hexagonal and square arrays have been extremely dependent on experimental conditions such as nanoparticle shape and size, array symmetry, particle concentration, and deposition methods on substrate.¹³⁻¹⁸ Theoretical calculations¹⁹⁻²¹ have been made in the past few years aiming to explain these formations. On several nanoparticle systems, the square \rightarrow hexagonal phase transformation occurs by the increase in colloidal concentration.^{18,22,23} In some oil-drop experiments, this can be achieved by increasing the vibrational frequency of bounce²⁴ while in 2D electronical crystals, with layered structures, it occurs by changing the interlayer distance.²⁵

In this work, we study a pressure-induced structural phase transition in a two-dimensional system. A modified interaction potential, which has the same functional form of the

potential proposed by Lee *et al.*,⁶ was used to study the structural phase transformation in a 2D system. This interaction potential is very rich since it reveals a vast phase diagram as it has been reported by Engel *et al.*²⁶ The 2D crystal, initially in a square structure, undergoes a transition to a hexagonal structure once we apply sufficient pressure onto the system. To this end, we use classical molecular dynamics in the isobaric-isoenthalpic ensemble²⁷ which permits us to observe structural changes in the material being simulated. Further discussion on the potential will be given on Sec. II. On our investigations, we made a preliminary analysis about the crystallization behavior of the system. We then studied the microscopic motion of the particles during the pressure-induced transition. The reverse transformation shows hysteresis and occurs at a certain range of temperature. At low temperatures, reversibility could be attained by applying negative pressure, as it was observed in the tridimensional system.⁶ We also obtained the minimum energy path for the square \rightarrow hexagonal transition using the nudged elastic band (NEB) method²⁸ in order to clarify the kinetic aspect of this transformation. Analogous structure transitions have been observed on several systems, particularly those involving self-assembled particles on substrate.^{8,10,22,24,25} On these systems, transformations can be obtained by changing experimental conditions such as density, pressure, temperature, and others.

The paper is organized as follows. In Sec. II we describe the system and the molecular-dynamics procedure. In Sec. III we discuss the computer experiments and our results. In Sec. IV we finally conclude.

II. MODEL AND SIMULATION PROCEDURE

Based on the interaction potential proposed by Lee *et al.*,⁶ we consider the modified Lennard-Jones potential in order to favor a square lattice in a 2D system. This choice is necessary to make a less compact system to be more stable at zero pressure, permitting us to observe possible phase transitions when pressure is applied. Indeed, a square lattice can never

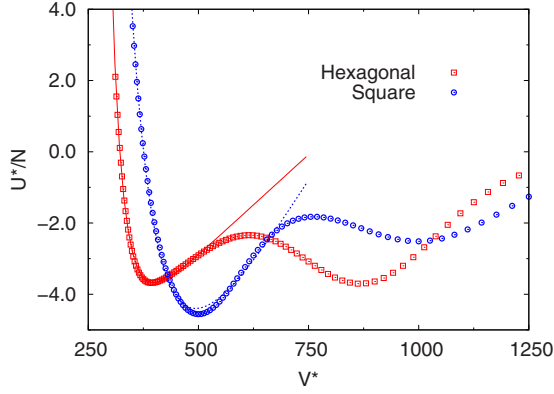


FIG. 1. (Color online) Cohesive energy per particle for square and hexagonal structures as a function of the reduced volume. Lines represent the curve fitting of the Murnaghan equation. The parameters for the square/hexagonal lattice are $B_0=0.138(3)/0.147(2)$, $B'_0=6.83(6)/12.96(15)$, $V_0=494.3(8)/398.9(4)$, and $E_0=-4.40(2)/-3.67(1)$.

be stable for potentials with the form $V(r)=A/r^n+B/r^m$ (Ref. 29). Other potentials, however, could be used for this purpose.^{30,31}

The expression for the modified Lennard-Jones potential is

$$V_{\text{MLJ}}(r) = -4\epsilon \left[\left(\frac{\sigma}{r} \right)^6 - \left(\frac{\sigma}{r} \right)^{12} \right] - G e^{-(r-r_0/\lambda)^2}. \quad (1)$$

The first term is the standard Lennard-Jones potential. The second term is introduced to make the square lattice more stable at zero pressure. G is the intensity of this interaction, λ is the width of the Gaussian function, and r_0 is the second neighbor distance. We then performed MD calculations in a 2D system containing 400 particles using the (N, P, H) ensemble²⁷ (number of particles, pressure, and enthalpy are constants during simulation). In this ensemble, the simulation box can change both size and shape, which makes it a useful tool to analyze structural changes throughout the simulation.

We solve the equations of motion using Gear's fifth-order predictor-corrector algorithm.³² Energy is in units of ϵ and length is in units of σ (Ref. 33). The potential was shifted at the cutoff $r_{\text{cut}}=4.5$ so the potential function and its derivative go smoothly to zero at r_{cut} (Ref. 34). In this work, $G=1.0$, $\lambda=0.2$, $r_0=1.6$, and a time step $\Delta t^*=1.0 \times 10^{-2}$. All physical quantities are in reduced units and are indicated by an asterisk.

The lattice energy for each structure as a function of the reduced volume and the Murnaghan equation of state curve fit are shown in Fig. 1. The Murnaghan equation is defined as³⁵

$$E(V) = E_0 + \frac{B_0 V}{B'_0} \left(\frac{(V_0/V)^{B'_0}}{B'_0 - 1} + 1 \right) - \frac{B_0 V_0}{B'_0 - 1}, \quad (2)$$

where B_0 and B'_0 are the zero-pressure bulk modulus and its pressure derivative; V_0 and E_0 are the volume and energy of the relaxed state.

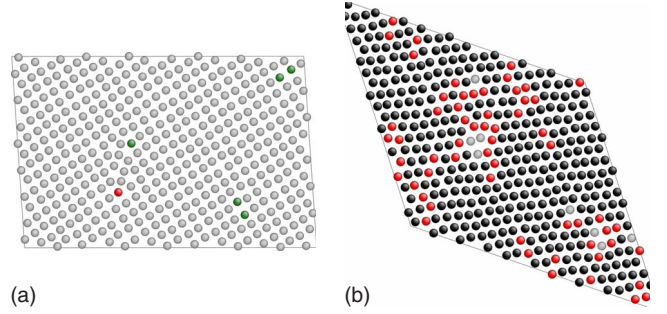


FIG. 2. (Color online) Snapshots of the system after crystallization: (a) $P^*=1$; (b) $P^*=4$. In both cases, almost no defect was formed. Colors indicate the coordination number of each particle (green=3, grey=4, red=5, and black=6).

III. RESULTS AND DISCUSSION

A. Melting and crystallization

The system was setup initially at fixed $P^*=1$ with density $\rho^*=0.8$ and at temperature $T^*=10^{-3}$ in a square structure. We then increased the temperature at the rate of 0.03 each 2×10^4 time steps. By investigating the system density as a function of temperature we could find the approximate melting point at $T^*=0.59$. The liquid system was then cooled at the same rate. As a result, the melt crystallized in the square structure with little formation of defects, as shown in Fig. 2(a). All snapshots were generated using the ATOMEYE atomistic configuration viewer of Li.³⁶

Next, we heated the initial crystal at the rate of 0.05 each 2×10^4 time steps at fixed pressure $P^*=4$. When the system reached $T^*=0.05$, it was found to be in a hexagonal structure due to the pressure applied (details in the following subsections). The system melted at $T^*=0.95$ at this pressure and showed crystallization to the hexagonal structure when cooled at the same rate [Fig. 2(b)] again with little formation of defects.

B. Structural transitions at low temperatures

Our preliminary goal was to identify at which pressure the initial square lattice transforms to a hexagonal one at low temperatures. We set the temperature of the system at $T^*=10^{-3}$ and we applied pressure at a rate of 0.1 pressure units each 2×10^4 time steps. The structural phase transition was observed at $P^*=5.4(1)$. This is a first-order phase transition and was clearly identified by a jump of the system density.

We were not able to find the reverse transition for this system at low temperatures, even at zero pressure and with large period of thermalization. Reversibility could only be achieved when tension outward the system, i.e., negative pressure, was applied. In other words, the system could self-assemble into a square symmetry when we allowed a larger area for the particles to move in. This process is described in Fig. 3. This reverse transition has an analogous phenomenon occurring in the 3D system studied by Lee *et al.*⁶ at low temperatures using the same form of potential.

The impossibility to achieve the hexagonal \rightarrow square transition at low temperatures is due to the lack of kinetic energy necessary for the system to jump between the hexagonal and

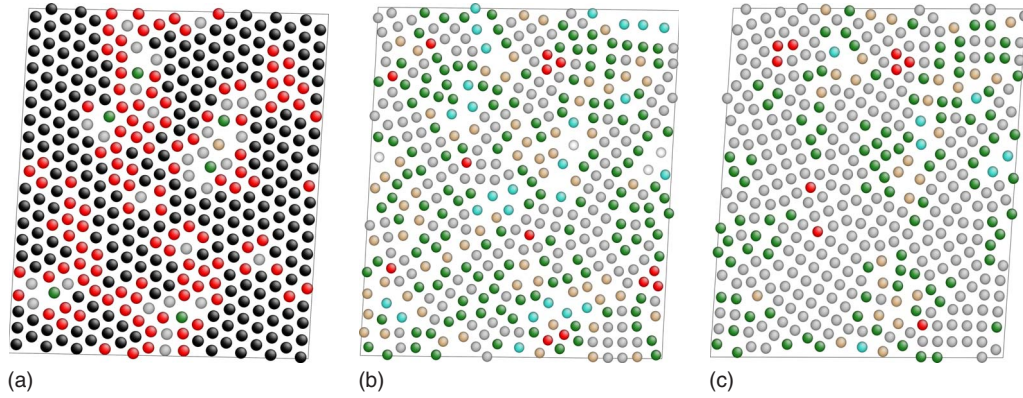


FIG. 3. (Color online) Snapshots of the system during the hexagonal \rightarrow square transition induced by negative pressure. In (a), small defects arise from the initially perfect hexagonal structure at $P^* = -1.71(1)$. The system evolves into a rarified state (b) when equilibrium is reached. Finally in (c) tension is removed: the system exhibits formation of domains in the square structure. Colors as in Fig. 2.

the square cohesive energy wells for system volumes below 600 (see Fig. 1).

C. Structural transitions near the melting point

Differently from the low temperature case, for systems with high temperatures, e.g., near the melting point, the reverse transition would be feasible. The square lattice was then heated at fixed zero pressure until melting occurred at

$T^* = 0.43(1)$. We set the temperature of the system at $T^* = 0.4$ (93% of the estimated melting temperature³⁷) and performed the same procedure done at a low temperature. This time, the system went from square to hexagonal symmetry at $P^* = 2.8(1)$. A short pretransformation stage was identified when the pressure reached $P^* = 2.6$ as shown in Fig. 4(a). In this stage, the system is no longer a perfect square lattice and shows sliding between two square domains (stacking fault line). From this point, if we reduce the pressure the system

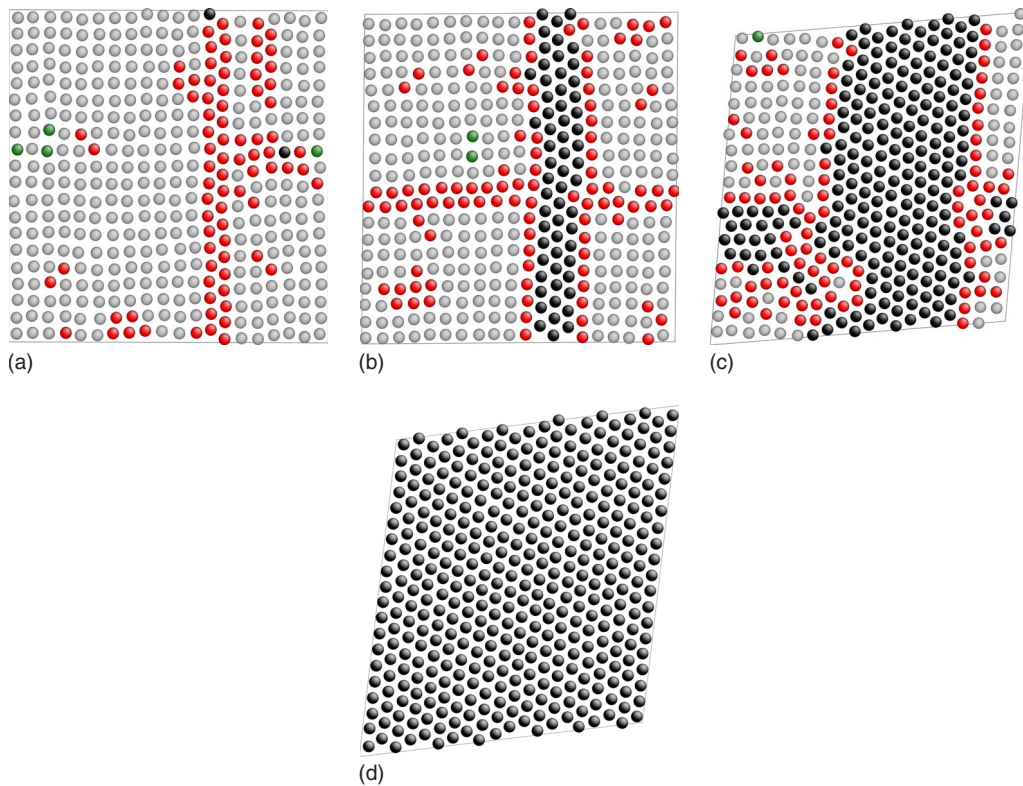


FIG. 4. (Color online) Snapshots of the system during the square \rightarrow hexagonal transition induced by pressure near the melting point. (a) The system exhibits sliding between two square domains at $P^* = 2.6$. (b) At time step 4000 and $P^* = 2.8$. The system starts to form a hexagonal “cross” inside the square lattice. (c) At time step 10 000 and $P^* = 2.8$. From this picture, it is clear the coexistence of two distinct phases and that there was no amorphization during the transition. (d) At time step 16 000 and $P^* = 2.8$, the system becomes a perfect hexagonal crystal. Colors as in Fig. 2.

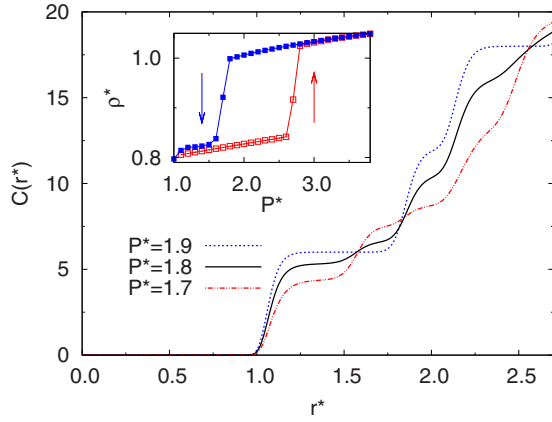


FIG. 5. (Color online) Pair coordination function for three values of pressure during the reverse transformation at $T^*=0.4$. (Inset) Reduced density as a function of P^* . Open squares indicate increase in pressure. Filled squares indicate the reverse process.

returns to a perfect square lattice. At low temperatures, the pretransformation stage was not identified in the square \rightarrow hexagonal transition, which differs from the three-dimensional case.⁶ Moreover, Fig. 4 shows how the particles rearrange during the square \rightarrow hexagonal transition. In this transition, there is the coexistence of both square and hexagonal structure before the system finally crystallizes into a perfect hexagonal symmetry.

The system went back to square symmetry at $P^*=1.6(1)$ showing hysteresis during the transformation. The coordination number during decrease in pressure (Fig. 5) shows that the system passes from a hexagonal structure (coordination number equal 6) to a square structure (equal 4). In this reverse transformation, showed in Fig. 6, we first observe some defect formation with no apparent crystallization. As the system evolves, it slowly changes to an amorphous state before finally having a square symmetry with the formation of two domains.

The hexagonal \rightarrow square transition differs from the square \rightarrow hexagonal transition in some aspects. The reverse transition takes a longer time to complete than the square \rightarrow hexagonal one. Also, we observed amorphization only during the reverse transition. These two aspects are probably related since a high atomic mobility and a larger area for the atoms to move are required for the reverse transition to be possible. The high mobility of the particles can lead to an amorphization. Thus, a longer time would be necessary for the particles to rearrange themselves into a new stable structure.

Those transitions are uniquely dependent on the thermodynamic state of the system. In other words, if we keep the pressure fixed and increase the temperature, the square \rightarrow hexagonal transformation occurs, as is exemplified in Fig. 7. However, the reverse transformation could not be achieved since a high mobility of the atoms is necessary for such transition.

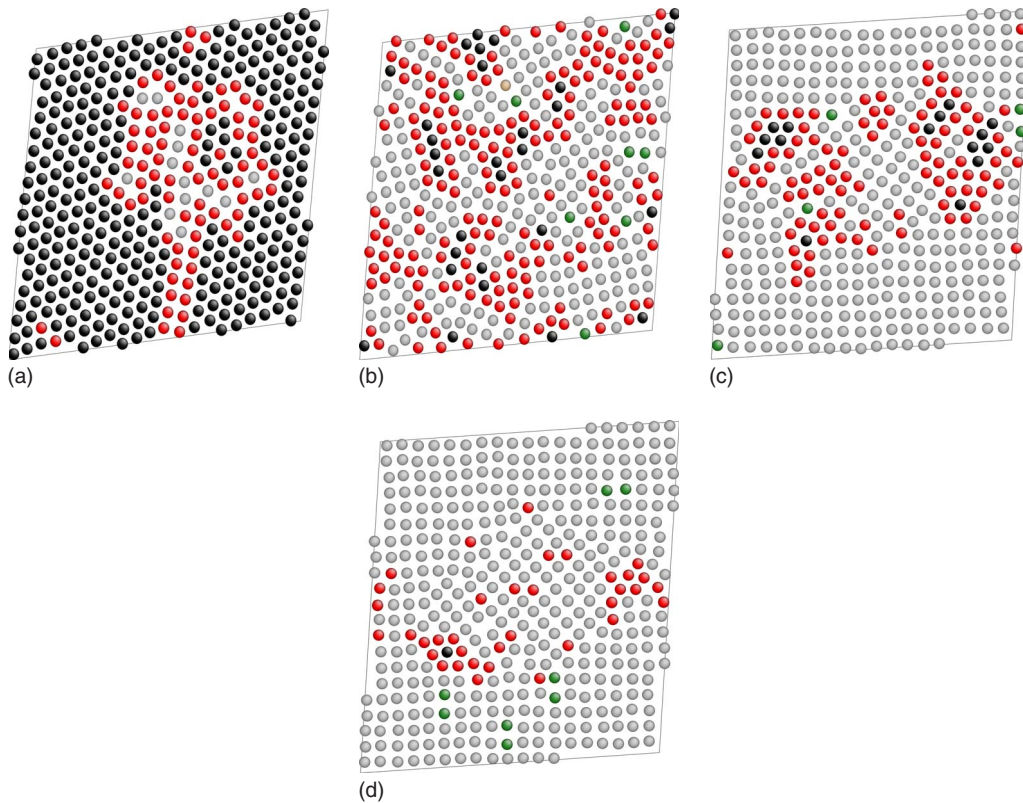


FIG. 6. (Color online) Snapshots of the system during the hexagonal \rightarrow square transition induced by decrease in pressure near the melting point. (a) At time step 9000 and $P^*=1.6$. The system exhibits some formation of defects in the hexagonal lattice. (b) At time step 21 000 and $P^*=1.6$. The system becomes temporarily amorphous due to the high mobility of the atoms. (c) At time step 36 000 and $P^*=1.6$. (d) At time step 42 000 and $P^*=1.6$, we have the formation of two domains in a square symmetry. Colors as in Fig. 2.

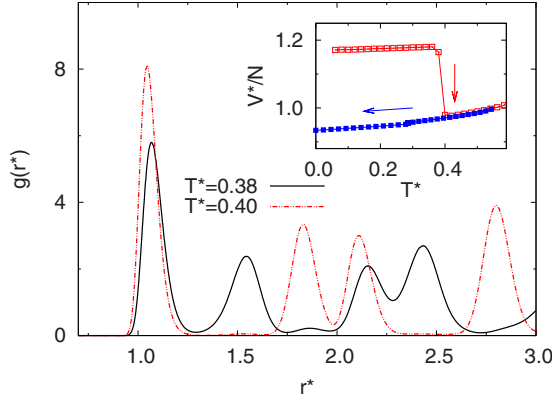


FIG. 7. (Color online) Pair distribution function for two states during temperature-induced phase transition at fixed $P^*=4$. (Inset) Atomic volume as a function of T^* . Arrows indicate the sense of the transition.

D. Transitional energy barrier and phase diagram

The evaluation of the activation energy barrier for a square \rightarrow hexagonal transition was made using the NEB method.²⁸ This is an efficient tool for finding the minimum energy path (MEP), given the knowledge of both the initial and final states. We used screenshots in the MD run during the transition at $T^*=0.05$ as the initial set of configurations (images). The algorithm converged after 90 000 iterations for a set of 13 images. We were then able to plot the enthalpy difference $\Delta H^* = H_{\text{image}}^* - H_{\text{square}}^*$ as a function of the reaction coordinate S_M defined as³⁸

$$S_M = \sum_{m=1}^M \sqrt{\sum_{i=1}^N (r_{i,m} - r_{i,m-1})^2} / N, \quad (3)$$

where N is the number of particles, M is the number of images, and r is the atomic coordinate in the configuration phase space. The activation energy found in the MEP (Fig. 8) is equal to 0.11. We also calculated the MEP using screenshots of the transition at $T^*=0.30$ as the initial set of images. The MEP for this case yielded the same result for the activation energy, as expected from transition kinetics theory (see Ref. 39, for example).

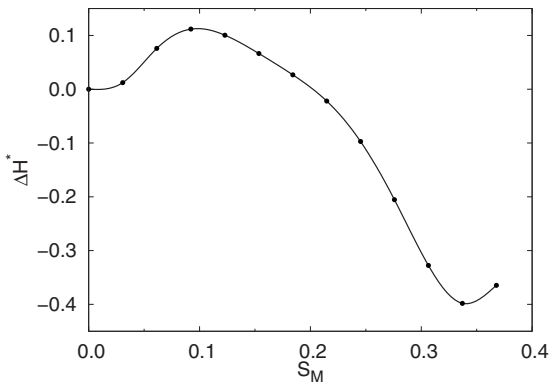


FIG. 8. The minimum energy path for the square \rightarrow hexagonal transition. Points are connected via cubic spline interpolation.

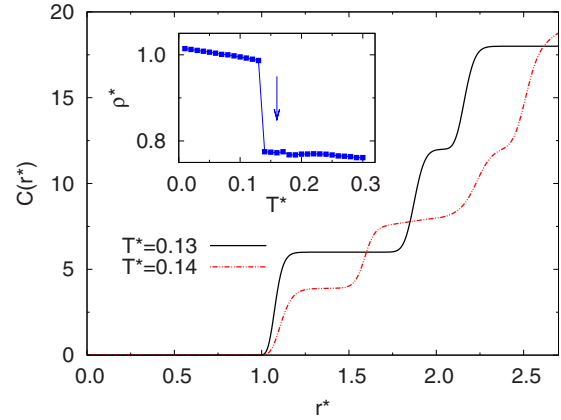


FIG. 9. (Color online) Pair coordination function for two states during increasing temperature phase transition at fixed $P^*=0$. (Inset) Reduced density as a function of T^* . The density drop indicates the minimum temperature for the hexagonal \rightarrow square transition.

Another notable property of the system is the minimum temperature necessary for the occurrence of hysteresis. We started with the system in a hexagonal structure at $T^*=0.01$, i.e., the low temperature regime, and $P^*=6.0$. We then decreased the pressure until $P^*=0$. The system remained in a hexagonal structure as expected. Later, while keeping zero pressure, we heated the system until it passed from the hexagonal to the square symmetry at $T^*=0.14$, as can be observed in Fig. 9. The transition temperature here reported can be regarded as a lower limit for the occurrence of hysteresis in this type of pressure-induced phase transition.⁴⁰

Additionally, we performed some simulations to construct a $P \times T$ phase diagram (Fig. 10) in order to clarify the equilibrium phases of a given thermodynamic state. To create the square-hexagonal coexistence curve, we identified at which pressure the system went from a square structure to a hexagonal one on each temperature. At temperatures above 0.45, a hybrid phase was found in which both square and hexagonal domains coexisted even for long periods of thermalization. We believe this behavior is due to the formation of defects in the square lattice at high temperatures. We were able to construct the phase diagram up to $T^*=0.58$. At higher temperatures, data were not reproducible due to the difficulty to simulate the liquid state in the (N, P, H) ensemble.

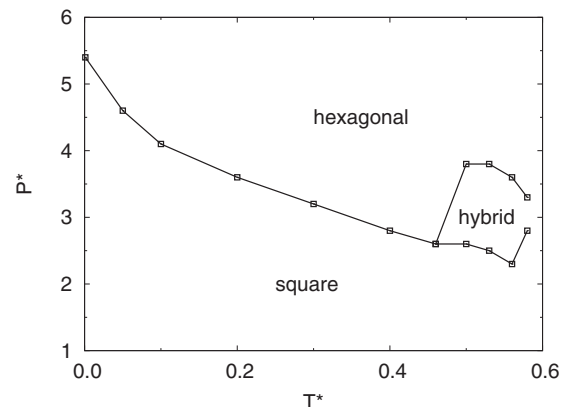


FIG. 10. Phase diagram of the system.

IV. CONCLUSIONS

In this work, we have studied in detail the mechanisms of pressure-induced phase transitions using MD techniques. The particles in the 2D system interacted via a modified Lennard-Jones potential. We examined the conditions at which a structural transition was possible for different temperatures and pressures applied.

The crystallization behavior of the system showed a strong dependence with the pressure applied. For low values of P^* , the melted system crystallizes in the square structure and for higher values, it rearranges into the hexagonal structure.

In regard to the main focus of the paper, we observed two distinct behaviors for pressure-induced phase transitions. At low temperatures, we concluded that the square \rightarrow hexagonal transition is irreversible unless we apply a negative pressure onto the system. For temperatures above

$T^*=0.14$, the transition is reversible and shows hysteresis.

The dynamics observed in these transitions are similar to those occurred in several systems, particularly those involving self-assembled particles on substrate. As an example, in systems of inclusions over liquid crystals, the application of lateral pressure causes the system to self-organize into a more compact structure⁴¹ (long chains \rightarrow square \rightarrow hexagonal). Like our systems, increase in temperature and density has the same effect of producing such transitions.

ACKNOWLEDGMENTS

The authors would like to thank the Coordenação de Aperfeiçoamento de Pessoal de Nível Superior (CAPES), the Conselho Nacional de Desenvolvimento Científico e Tecnológico (CNPq), and the Fundação de Amparo à Pesquisa do Estado de São Paulo (FAPESP) for financial support.

*djpr@df.ufscar.br

- ¹L. Dubrovinsky, N. Dubrovinskaia, O. Narygina, I. Kantor, A. Kuznetsov, V. B. Prakapenka, L. Vitos, B. Johansson, A. S. Mikhaylushkin, S. I. Simak, and I. A. Abrikosov, *Science* **316**, 1880 (2007).
- ²A. B. Belonoshko, R. Ahuja, and B. Johansson, *Nature (London)* **424**, 1032 (2003).
- ³L. Vocadlo, D. Alfè, M. J. Gillan, I. J. Wood, J. P. Brodholt, and G. D. Price, *Nature (London)* **424**, 536 (2003).
- ⁴J. F. Lin, V. V. Struzhkin, W. Sturhahn, E. Huang, J. Zhao, M. Y. Hu, E. Alp, H. K. Mao, N. Boctor, and R. J. Hemley, *Geophys. Res. Lett.* **30**, 2112 (2003).
- ⁵J.-F. Lin, D. L. Heinz, A. J. Campbell, J. N. Devine, and G. Shen, *Science* **295**, 313 (2002).
- ⁶K. Y. Lee and J. R. Ray, *Phys. Rev. B* **39**, 565 (1989).
- ⁷H. Mao, W. A. Bassett, and T. Takahashi, *J. Appl. Phys.* **38**, 272 (1967).
- ⁸L. Zhou and Y. Ma, *J. Phys.: Condens. Matter* **20**, 095006 (2008).
- ⁹T. Okubo, *J. Chem. Phys.* **87**, 5528 (1987).
- ¹⁰P. Cluzeau, P. Poulin, G. Joly, and H. T. Nguyen, *Phys. Rev. E* **63**, 031702 (2001).
- ¹¹V. G. Nazarenko, A. B. Nych, and B. I. Lev, *Phys. Rev. Lett.* **87**, 075504 (2001).
- ¹²S. C. Glotzer and M. J. Solomon, *Nature (London)* **6**, 557 (2007).
- ¹³J. C. Swarbrick, J. Ma, J. A. Theobald, N. S. Oxtoby, J. N. O'Shea, N. R. Champness, and P. H. Beton, *J. Phys. Chem. B* **109**, 12167 (2005).
- ¹⁴M. Tanaka, N. Shimamoto, T. Tanii, I. Ohdomari, and H. Nishide, *Sci. Technol. Adv. Mater.* **7**, 451 (2006).
- ¹⁵S. Egusa, P. L. Redmond, and N. F. Scherer, *J. Phys. Chem. B* **111**, 17993 (2007).
- ¹⁶P. Cluzeau, G. Joly, H. T. Nguyen, and V. K. Dolganov, *JETP Lett.* **75**, 482 (2002).
- ¹⁷P. V. Dolganov, E. I. Demikhov, V. K. Dolganov, B. M. Bolotin, and K. Krohn, *Eur. Phys. J. E* **12**, 593 (2003).
- ¹⁸V. K. Dolganov and S. P. Palto, *Phys. Usp.* **48**, 743 (2005).
- ¹⁹C. Bohley and R. Stannarius, *Eur. Phys. J. E* **23**, 25 (2007).
- ²⁰P. V. Dolganov, H. T. Nguyen, G. Joly, V. K. Dolganov, and P. Cluzeau, *Europhys. Lett.* **78**, 66001 (2007).
- ²¹J. Fukuda, *Eur. Phys. J. E* **24**, 91 (2007).
- ²²C. L. Ren and Y. Q. Ma, *J. Am. Chem. Soc.* **128**, 2733 (2006).
- ²³Z. Zhou, Q. Yan, Q. Li, and X. S. Zhao, *Langmuir* **23**, 1473 (2007).
- ²⁴S. I. Lieber, M. C. Hendershott, A. Pattanaporkratana, and J. E. MacLennan, *Phys. Rev. E* **75**, 056308 (2007).
- ²⁵G. Goldoni and F. M. Peeters, *Phys. Rev. B* **53**, 4591 (1996).
- ²⁶M. Engel and H.-R. Trebin, *Phys. Rev. Lett.* **98**, 225505 (2007).
- ²⁷M. Parrinello and A. Rahman, *Phys. Rev. Lett.* **45**, 1196 (1980).
- ²⁸H. Jónsson, G. Mills, and K. W. Jacobsen, in *Classical and Quantum Dynamics in Condensed Phase Simulations*, edited by B. J. Berne *et al.* (World Scientific, Singapore, 1998).
- ²⁹K. Zabinska, *Phys. Rev. B* **43**, 3450 (1991).
- ³⁰A. J. C. Ladd and W. G. Hoover, *J. Chem. Phys.* **74**, 1337 (1981).
- ³¹L. L. Boyer, *Phys. Rev. B* **53**, 3145 (1996).
- ³²D. Beeman, *J. Comput. Phys.* **20**, 130 (1976).
- ³³L. Verlet, *Phys. Rev.* **159**, 98 (1967).
- ³⁴M. P. Allen and D. J. Tildesley, *Computer Simulation of Liquids* (Oxford University Press, USA, 1989).
- ³⁵F. D. Murnaghan, *Proc. Natl. Acad. Sci. U.S.A.* **30**, 244 (1944).
- ³⁶J. Li, *Model. Simul. Mater. Sci. Eng.* **11**, 173 (2003).
- ³⁷The rational melting temperature can be obtained, for example, by the coexistence method [E. T. Chen, R. N. Barnett, and U. Landman, *Phys. Rev. B* **40**, 924 (1989)]. The rather crude estimate for the melting temperature done in this paper had the purpose to find a high temperature scale for the system in the solid state.
- ³⁸O. Trushin, E. Granato, S. C. Ying, P. Salo, and T. Ala-Nissila, *Phys. Rev. B* **68**, 155413 (2003).
- ³⁹K. J. Laidler, *Theories of Chemical Reaction Rates* (McGraw-Hill, USA, 1969).
- ⁴⁰C. N. R. Rao and K. J. Rao, *Phase Transitions in Solids* (McGraw-Hill, USA, 1978).
- ⁴¹P. Cluzeau, G. Joly, H. T. Nguyen, and V. K. Dolganov, *JETP Lett.* **76**, 351 (2002).